IEEE Access
Multidisciplinary | Rapid Review | Open Access Journal

Received 14 July 2022, accepted 2 August 2022, date of publication 5 August 2022, date of current version 11 August 2022.

Digital Object Identifier 10.1109/ACCESS.2022.3196641

RESEARCH ARTICLE

Low Complexity Non-Uniform FFT for Doppler Compensation in OFDM-Based Underwater Acoustic Communication Systems

VAN DUC NGUYEN, HOAI LINH NGUYEN THI, QUOC KHUONG NGUYEN, AND TIEN HOA NGUYEN

School of Electronics and Telecommunications, Hanoi University of Science and Technology, Hanoi 100000, Vietnam

Corresponding author: Tien Hoa Nguyen (hoa.nguyentien@hust.edu.vn)

This work was supported by the Vietnams National Foundation for Science and Technology Development (NAFOSTED) under Grant 102.04-2018.12.

ABSTRACT The Doppler effect critically degrades the performance of orthogonal frequency division multiplexing (OFDM) systems in general. This problem is significantly worse for underwater acoustic (UWA) communication systems due to the distinct characteristics of the underwater channel, resulting in the loss of orthogonality among sub-carriers. In order to compensate Doppler shifts, including phase noise and multipath channels in realistic communication scenarios, the joint of channel estimation and ICI reduction is often performed. However, the accuracy depends on the channel estimation and the FFT size, while this leads to increased computational complexity at the receiver. To achieve this dual goal in the actual underwater communication environment, a novel pilot structure in the frequency domain has been applied to overcome the channel impulse response (CIR) variation in a block period. The coarse Doppler shift is firstly estimated by using the received pilot signal. Afterward, the study takes advantage of the flexibility provided by non-uniform fast Fourier transform (NFFT) in choosing the sampling points to construct a fast and stable Doppler frequency Compensation Matrix-based NFFT (DCMN) to fine compensate the Doppler phase shift. Finally, this study shows the improvement of the proposed method's performance by actual experimental measurements and simulations.

INDEX TERMS Doppler frequency shift estimation and compensation, interchannel interference, non-uniform fast Fourier transform, OFDM, underwater acoustic communications.

I. INTRODUCTION

In the past decade, underwater communications (UWA) using orthogonal frequency division multiplexing (OFDM) have received remarkable interest both in research as well as in industry with a wide range of military and civilian applications [1], [2]. Nevertheless, the unique properties of the UWA channel, such as the slow propagation speed of the acoustic wave, the narrow bandwidth, and the time-varying multipath effect, that hinders the enhancement of the communication quality [3]. OFDM has been successfully applied in broadband wireless communication over time-varying radio channels [4]. Therefore, it is obviously appropriate to continue using OFDM for UWA systems to combat the multipath effect as well as improve the transmission rate [5]. However, the using OFDM to UWA presents its own challenges, especially since the low available bandwidth is not negligible compared to the center frequency, resulting in an un-uniform Doppler shift among sub-carriers causing significant inter-carrier interference (ICI) problem [6], [7]. Moreover, the problem of OFDM signal synchronization as well as the high sensibility of UWA systems with the carrier frequency offset (CFO) is also a big challenging task [8]. CFO and doubly selective fading channels impose additional challenges to the synchronization problem as a direct consequence of Doppler spread [9]. Thus the idea of pilot designs with guard

The associate editor coordinating the review of this manuscript and approving it for publication was Wei Jiang.

symbols to combat ICI in the frequency domain and inter-symbol interference (ISI) in the time domain has been greatly restricted [10].

Many studies have shown that to improve the performance of UWA-OFDM systems, it is necessary to effectively handle the Doppler shift (and also the CFO) through accurate channel estimation and ICI cancellation [11], [12].

Nowadays, there are a large number of research works on channel estimation and ICI cancellation problems have been published [13], [14]. It cannot be denied that by mining big data, machine learning (ML) or AI play a very important role in handling these two problems [15]. However, in order to have diverse measurement results, most of recent studies use channel modeling, instead of having actual measurement results [16], [17].

We focus on pilot-based channel estimation methods, similar to those of the UWA-OFDM studies that appear for example in [18]. Continuing with the problem of time-frequency doubly-selective channel estimation, the solution of insert pilots in both time and frequency domains is applied [4]. In the many literature, pilots will first be used for CFO correction, and then offset-corrected signals will be used for channel estimation [19]. However, the assumption that the receiver will feedback to the transmitter about channel state information (CSI), such as in terrestrial applications, is no longer valid in underwater communications [20]. Because the coherent time of the acoustic channel is much shorter than the time it takes for the signal traveling from the transmitter to the receiver with a distance of about 1km. Therefore, using training sequences will certainly not be effective. Instead, some studies use cyclic prefix (CP) as a preamble to handle with the problem of Inter-symbol interference (ISI), and to do synchronization of the UWA-OFDM system [21]–[23].

The zero-padded (ZP)-OFDM method with zero overlap has been shown to be more efficient than the CP-OFDM method in underwater communications [24], [25]. Because devoting power to useful signals while not wasting energy on redundant CP for long and stable transmission is more important than improving transmission rates in UWA applications [26]. Today, several companies offer commercial underwater sonar devices that support different data rates for different ranges [27]. The trade-off between data rates and ranges depends on the application requirements of the research [28]. The author in [29] has transmitted texts with a low data rate over a distance of several kilometers in harbour transmission scenario. The Bilkent University research team performed a bit rate transmission of 13.92 kbps at a distance of 7 meters [30]. Nowadays, the number of published studies on test-bed of underwater communication is very limited because of the aforementioned difficulties [31]. The existing literature on UWA-OFDM mainly uses underwater channel models and focuses on system analysis and simulation-based evaluation [32].

In this paper, we design a UWA-OFDM system using Beethoven's hydrophone with a transmission distance of over 1km. The main contributions and novelties are given as:

- We propose to increase the transmit power at one pilot (called pilot carrier frequency - PCF) by 1.5 times compared to the other sub-carriers. These increased power must, on the one hand, not be too large to ensure that the transmit signal is not distorted after amplified up to 500W, and on the other hand to ensure efficient re-modulation at the receiver. Hence, the PCF is used to determine the Doppler frequency shift (including CFO). This approach is completely different from previous studies that divide the transmit power uniformly among all pilots sub-carriers. We then used time-domain resampling, which has been a very powerful tool to alleviate nonuniform Doppler shifts [26].
- Similar to other conventional two-step approaches to alleviate the Doppler effect, the coarse- and the fine compensation phase will be used to compensate CFO and Doppler shifts, respectively [33], [34]. As illustrated in [33], the resampling besides being effective in non-uniform Doppler shift compensation, will increase the FFT size significantly. Agreed, the oversized FFT problem is theoretically still be accurately handled through digital signal processing [26]. However, the utilization of the ICI matrix inversion with the computational complexity of $O(N^2)$ will be a problem at the receiver [34]. The main difference of this study is to use non-uniform fast Fourier transform (NFFT) in choosing the sampling points to construct a fast and stable Doppler frequency Compensation Matrix-based NFFT (DCMN) to fine compensate the Doppler phase shift. By doing so, we have combined the IFFT operation with the Doppler frequency compensation. Thus, the receiver complexity of our proposal is significantly reduced when compared with the state of the art [34], [39].
- The remaining contribution of this study is to present a test-bed UWA-OFDM with a transmission distance of more than 1km. The system has been tested on many rivers and lakes with a depth of several tens of meters, and the experimental results have proven the stability of the proposed method.

The rest of the paper is organized as follows. In section II, we discuss about the data structure and propose a fast and stable Doppler frequency Compensation Matrix-based NFFT to compensate the Doppler phase shift. In section III, we describe the experiment setting. We provide experimental results and discussions in section IV. System performance evaluation by simulation is given in section V. Finally, we conclude the paper in section VI.

Notation: Lower boldface letters denote column vectors. The superscript $(\cdot)^*$, $(\cdot)^T$, $(\cdot)^H$ stands for the conjugate, transpose, and conjugate-transpose operator, respectively. The Euclidean norm and the expectation operators are denoted by $\|\cdot\|$ and $\mathbb{E}\{.\}$ respectively. $[a\, b]$ is denoted the join of 2 matrices in the column direction. Finally, $\mathcal{CN}\left(0, \sigma^2\right)$ denotes a circularly symmetric complex Gaussian distribution with zero mean and variance σ^2 and $\mathcal{N}\left(0, \sigma^2\right)$ denotes a Gaussian distribution.

II. DCMN ARCHITECTURE FOR DOPPLER COMPENSATION IN UWA-OFDM

With the main purpose of building a real-time underwater communication system, this study proposes a fast and stable Doppler frequency Compensation Matrix-based NFFT (DCMN) to fine compensate the Doppler phase shift. Whereas, the practical factors must be taken into account including transmission distance greater than 1km, transmission medium with many ravines, as well as system must work well with available hardware. The architecture of OFDM-based UWA communication systems is depicted in Fig. 1. At the receiver, the course Doppler shift is compensated in the first step. The DCMN, which combines the FFT transformation with the fine Doppler phase shift compensation, is conducted in the second step.

A. PILOTS AND DATA STRUCTURE OF TRANSMITTER SYSTEM MODEL

This paper uses the ZP-OFDM model as has been explained in detail in other experimental studies. The transmission model is designed to generate a real-time bandpass transmitted signal $x^{(n)}(t)$, where n is the sequence number of the OFDM frame. The OFDM frame structure is depicted in Fig. 2, where each OFDM frame consists of N_s ZP-OFDM. Let T_g denotes the duration of ZP, T represents the duration of one OFDM symbol, then we have a relationship $\Delta f = \frac{1}{T}$ with Δf is the sub-carrier spacing. With the preamble D_z, where D_z interval acts as a pause interval, on the one hand to cancel the long echos, and on the other hand used to synchronize each OFDM frame. Thus, the duration of an OFDM Frame denoted by T_s is given as follows

$$T_s = N_s(T + T_g) + D_z \tag{1}$$

It is worth mentioning that we are talking about underwater channels with latency up to several hundred milliseconds. Therefore, the usual guard intervals are not sufficient. In this study, we have designed the OFDM frame structure from several possible experimental values and experimental models.

OFDM systems are considered susceptible to radio front-end induced impairments [35]. The OFDM-UWA system is especially susceptible to radio front-end induced impairments. This leads to the In-phase (I) and Quadrature (Q) phase branches from the transmitter itself becoming unbalanced. Furthermore, the nature of UWA channel properties is to hinder radio transmission, making it more difficult to synchronize the I/Q signal as well as the decoded signal at the receiver. Although, achieving the perfect balance between I/Q requires expensive analog hardware.

Without sacrificing generality, we use a solution that uses cheaper hardware. Specifically, we take advantage of the symmetry of the spectrum after the IFFT to modulate and transmit only the Q-signal branch. Thereby, we can eliminate the expensive analog part. To do so, there will be K pair of complex conjugated data symbol are transmitted simultaneously through each pair of symmetry sub-carriers in a ZP-OFDM. Here, data means either useful data or pilots. Considering in a ZP-OFDM, let $d_i(k)$ denote the k^{th} data symbol at i^{th} sub-carrier, $k \in [1, \ldots, K], i \in [1, \ldots, N_{\text{FFT}}-1]$, with N_{FFT} is the length of IFFT. Since the sampling frequency of the audio signal f_s is usually chosen to be 96kHz. Whereas the bandwidth of the signal 12kHz. We need to insert $6K-2$ zeros symmetrically into vector $\boldsymbol{d}$ given in Eq. (2). The sub-carrier in the frequency domain p^{PCF}_{2K-1} is transmitted with a high power pilot signal for coarse estimation of the Doppler shift.

The following modulated QPSK symbols vector is defined

$$\boldsymbol{d} = \begin{bmatrix} [0_0, \ldots 0_{2K-2}]^T \\ p^{\text{PCF}}_{2K-1} \\ [d(1)_{2K}, \ldots, d(K)_{3K-1}]^T \\ [0_{3K}, \ldots, 0_{5K}]^T \\ [d^*(K)_{5K+1}, \ldots, d^*(1)_{6K}]^T \\ p^{*\text{PCF}}_{6K+1} \\ [0_{6K+2}, \ldots, 0_{8K-1}]^T \end{bmatrix} \tag{2}$$

Now let's interpret the Eq. (2), with $N_{\text{FFT}} = 2048$, and a total of $2K+2, (K = 256)$ sub-carriers are modulated by the data as well as pilots. $6K-2$ sub-carriers will be filled by zeros. The $(2K-1)^{\text{th}}$ sub-carrier denoted by p^{PCF} is the special pilot whose transmit power is 1.5 times greater than the other sub-carriers.

The passband of OFDM signal is given as

$$s^{(i)}(t) = \frac{1}{N_{\text{FFT}}} \sum_{k=0}^{N_{\text{FFT}}-1} d_k^{(i)} e^{i2\pi(f_{\min}+k\Delta f)t}, \quad t \in [0, T], \tag{3}$$

with $f_{\min}$ is the lowest frequency of the useful signal band. Thus, the maximum frequency of the signal occupying the frequency range is

$$f_{\max} = f_{\min} + K\Delta f \tag{4}$$

B. COARSE AND FINE DOPPLER COMPENSATION METHOD

Channel estimation is the most challenging part of underwater communication as mentioned above. We use the traditional approach that the channel estimation is performed based on pilot symbols. According to our design, N_P of pilot symbols (in a total of $2K+2$ data sub-carriers) are inserted into the frequency domain to interpolate the channel response. Moreover, the paper proposes to use a pilot carrier frequency (p^{PCF}) which is identified by transmitting with a larger power in the frequency domain compared to other sub-carriers. By using this identifier, the Doppler frequency shift is estimated. As given in Eq. (2), the PCF pilot is inserted at the $(2K-1)^{\text{th}}$ sub-carrier of the transmitted OFDM signal. The transmitted signal is implemented as shown in Fig. 3.

Let $(p^{\text{PCF}}, p_1^{(i)}, p_2^{(i)}, \ldots, p_{N_P}^{(i)})$ denote the pilot symbols of i^{th} OFDM symbol. Let f^{offset} denote the difference between the received and transmitted frequencies. We define the normalized Doppler shift (that includes also the CFO) ϵ_k as a ratio

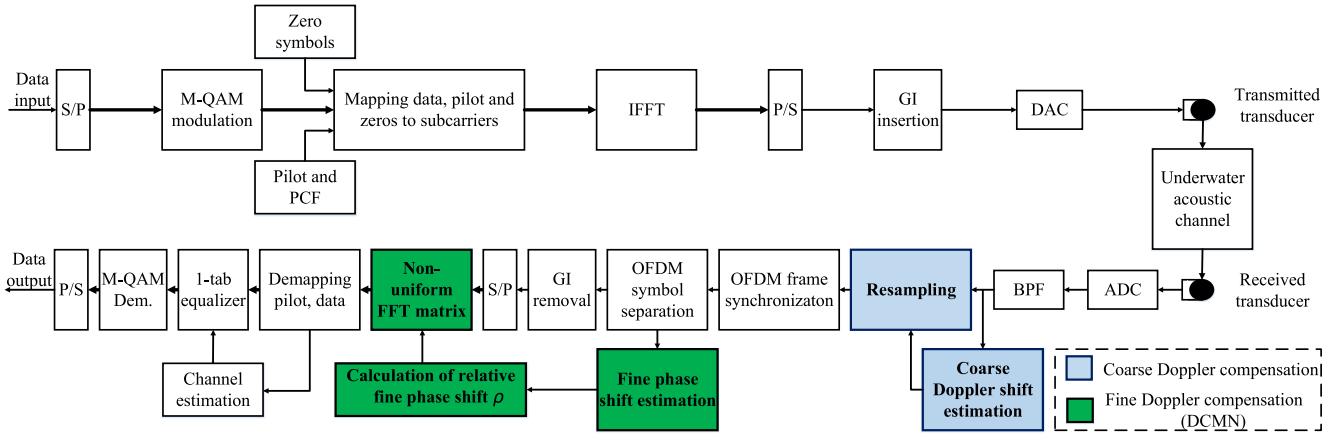

FIGURE 1. The structure of the underwater acoustic OFDM system using the DCMN to compensate the Doppler shift.

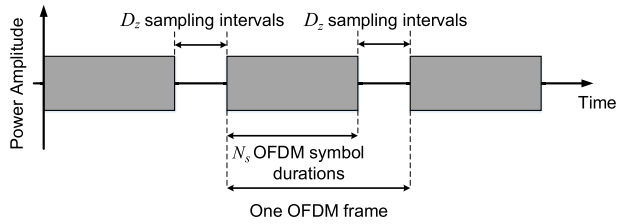

FIGURE 2. The OFDM frame structure in time domain.

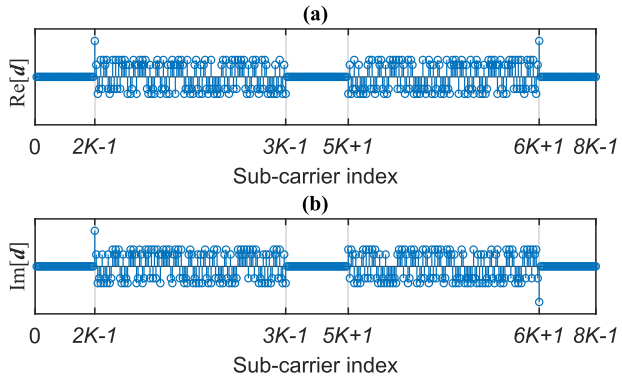

FIGURE 3. OFDM transmitted signal with practical considerations.

of the Doppler shift at k^{th} pilot symbol to sub-carrier spacing, shown as $\epsilon_k = \frac{f_k^{\text{offset}}}{\Delta f}$. To simplify the notation, we define the inserted pilots of i^{th} OFDM symbol:

$$\mathbf{P^{(i)}} = \begin{bmatrix} p^{\text{PCF}} & 0 & \cdots & 0 \\ 0 & p_1^{(i)} & & \vdots \\ \vdots & & \ddots & 0 \\ 0 & \cdots & 0 & p_{N_P}^{(i)} \end{bmatrix} \tag{5}$$

Without loss of generality, if we assume that only a Doppler shift (that also includes CFO) exists between transmitter and receiver. Since the PCF signal has a much larger power than other sub-carriers. Furthermore, the PCF pilot is broadcast at 12kHz. It will be easier to identify the PCF pilot at the receiver side. Then, the Doppler shift can be found from the first incoming PCF symbol. In order to reduce the Doppler effect, we can roughly compensate the factor ϵ^{PCF}. In other words, a large range of Doppler shift can be removed in the coarse synchronization step.

To be clear, let $\mathbf{D^{(i)}}$ denote the Doppler shift matrix after being compensated for frequency shift from PCF pilot as follows:

$$\mathbf{D^{(i)}} = \begin{bmatrix} 1 & 0 & \cdots & 0 \\ 0 & e^{\frac{2i\pi(\epsilon_1 - \epsilon^{\text{PCF}})}{N_{\text{FFT}}}} & & \vdots \\ \vdots & & \ddots & 0 \\ 0 & \cdots & 0 & e^{\frac{2i\pi(\epsilon_{N_P} - \epsilon^{\text{PCF}})}{N_{\text{FFT}}}} \end{bmatrix} \tag{6}$$

Given that the pilot channel gain is $\mathbf{H}_{\text{P}} = [H[p]]^T$, $p \in [\text{PCF}, 1, 2, \ldots, N_p]$, the received pilot signal of i^{th} OFDM symbol can be represented as

$$\mathbf{Y} = \mathbf{P^{(i)}}\mathbf{D^{(i)}}\mathbf{H}_{\text{P}} + \mathbf{N^{(i)}}, \tag{7}$$

where $\mathbf{N^{(i)}}$ represents the vector of Additive white Gaussian noise, with $\mathbb{E}\{\mathbf{N^{(i)}}[p]\} = 0$. In the following discussion let $\hat{\mathbf{H}}_{\text{P}} = \mathbf{D^{(i)}}\mathbf{H}_{\text{P}}$ denote the estimated channel gain that received by pilots. We simplify the least-square (LS) channel estimation method to estimate $\hat{\mathbf{H}}_{\text{P}}$ in such the way that the cost function $L(\hat{\mathbf{H}}_{\text{P}})$ is minimized as follows:

$$\begin{aligned} L(\hat{\mathbf{H}}_{\text{P}}) &= ||\mathbf{Y} - \mathbf{P^{(i)}}\hat{\mathbf{H}}_{\text{P}}||^2 \\ &= (\mathbf{Y} - \mathbf{P^{(i)}}\hat{\mathbf{H}}_{\text{P}})^H(\mathbf{Y} - \mathbf{P^{(i)}}\hat{\mathbf{H}}_{\text{P}}) \\ &= \mathbf{Y}^H\mathbf{Y} - \mathbf{Y}^H\mathbf{P^{(i)}}\hat{\mathbf{H}}_{\text{P}} - \hat{\mathbf{H}}_{\text{P}}^H\mathbf{P^{(i)}}^H\mathbf{Y} \\ &\quad + \hat{\mathbf{H}}_{\text{P}}^H\mathbf{P^{(i)}}^H\mathbf{P^{(i)}}\hat{\mathbf{H}}_{\text{P}} \end{aligned} \tag{8}$$

Next, we construct the derivative of the function of $L(\hat{\mathbf{H}}_{\text{P}})$ to zero,

$$\frac{\partial L(\hat{\mathbf{H}}_{\text{P}})}{\partial \hat{\mathbf{H}}_{\text{P}}} = -2(\mathbf{P^{(i)}}^H\mathbf{Y})^* + 2(\mathbf{P^{(i)}}^H\mathbf{P^{(i)}}\hat{\mathbf{H}}_{\text{P}})^* = 0 \tag{9}$$

It is clear that Eq. (9) gives the solution

$$\hat{\mathbf{H}}_{\mathrm{P}} = (\mathbf{P^{(i)}}^{H}\mathbf{P^{(i)}})^{-1}\mathbf{P^{(i)}}^{H}\mathbf{Y} = \mathbf{P^{(i)}}^{-1}\mathbf{Y} \tag{10}$$

It is worth mentioning that the phase shift is also a big problem in underwater communications. To understand the phase distortion in the received PCF signal, which is still remaining after the coarse synchronization step, let $\phi^{(i)}_{\mathrm{PCF}}$ denote the phase shift between two consecutive i^{th} and $(i+1)^{\mathrm{th}}$ OFDM symbol. $\phi^{(i)}_{\mathrm{PCF}}$ can be calculated bases on two identical consecutively transmitted signal $X_{(i)}$ and $X_{(i+1)}$ by a well-known approach [36] as:

$$\phi^{(i)}_{\mathrm{PCF}} = \frac{1}{2\pi} tan^{-1}\{\frac{\Im[X^{*}_{(i)}X_{(i+1)}]}{\Re[X^{*}_{(i)}X_{(i+1)}]}\} \tag{11}$$

Meanwhile, the phase shift is averaged over the entire transmission of one OFDM frame, which includes L OFDM symbols. Specifically, the fine phase shift is given as

$$\phi_{\mathrm{PCF}} = \frac{1}{L}\sum_{i=1}^{L}\phi^{(i)}_{\mathrm{PCF}} \tag{12}$$

The relative fine phase shift is then represented as

$$\rho = \frac{\phi_{\mathrm{PCF}} f_s}{(N_{\mathrm{FFT}} + GI)2\pi f_c} \tag{13}$$

where f_s represents the sampling frequency, f_c denotes the center frequency and GI stands for the guard interval length. Fig. 4 shows the particular phase noise with and without the fine compensation step.

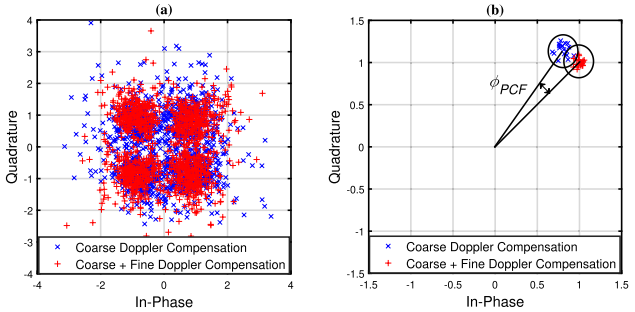

FIGURE 4. Coarse and fine doppler cancellation with PCF pilot.

At the receiver, the acoustic signal is received by the transducer, then it is amplified and converted to the digital signal by an ADC with the sampling frequency f_s. The band-pass filter (BPF) is used to eliminate the out-band noise. Due to the Doppler frequency shift that leads to a mismatch between the transmitter and receiver sampling clocks. Fig. 5 illustrates the mismatch between the transmitter and receiver oscillator clocks that causes the phase shift.

The frequency-domain received signal before fine phase shift compensation is continued to be written from Eq. 7 as

$$\tilde{\mathbf{Y}}_l[k] = \underbrace{\mathbf{Y}_l[k]\frac{sin(\pi\rho k)}{sin(\pi\rho k/N_{\mathrm{FFT}})}}_{\text{Received Amplitude}} \underbrace{e^{\frac{j\pi\rho k(l-1)}{N_{\mathrm{FFT}}}}}_{\text{Phase Distortion}} + z_l^{ICI}[k], \tag{14}$$

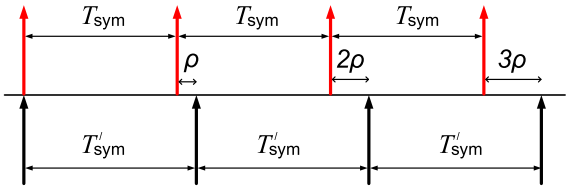

FIGURE 5. Effect of doppler shift in the re-sampling process.

where $z_l^{ICI}[k]$ represents the ICI interference at k^{th} sub-carrier of l^{th} OFDM symbol.

In the presence of Doppler shift, the sampling time varies within every OFDM symbol. Hence the problem of extracting the useful signal may occur in receiver samples. To suppress phase distortion on the one hand, and on the other hand to reduce ICI, we propose the $N_{\mathrm{FFT}} \times N_{\mathrm{FFT}}$ non-uniform FFT matrix $[\mathbf{G}_{\mathbb{RS}}]$, give as

$$[\mathbf{G}_{\mathbb{RS}}] = \begin{bmatrix} 0 & \cdots & 0 \\ \vdots & \ddots & \vdots \\ g_{2K-1,0} & \cdots & g_{2K-1,N_{\mathrm{FFT}}-1} \\ \vdots & \ddots & \vdots \\ g_{3K-1,0} & \cdots & g_{3K-1,N_{\mathrm{FFT}}-1} \\ 0 & \cdots & 0 \\ \vdots & \ddots & \vdots \end{bmatrix} \tag{15}$$

where

$$g_{k,n} = \begin{cases} e^{-\frac{j\pi\rho k(l-1)}{N_{\mathrm{FFT}}}} & \text{if } k \in [2K-1,\ldots,3K-1] \\ 0 & \text{else.} \end{cases}$$

To remove the ICI, we propose to form the non-uniform FFT matrix $[\mathbf{G}_{\mathbb{RS}}]$ with the size of N_{FFT}xN_{FFT} as depicted in Eq. (15). This matrix, known as the non-uniform FFT matrix, performs both the remaining Doppler frequency compensation and the FFT operation. As shown in Fig. 3, the sub-carriers reserved for data are from $2K-1$ to $3K-1$ and from $5K+1$ to $6K+1$, others are null sub-carriers. Moreover, the inserted data symbols in the sub-carrier position from $5K+1$ to $6K+1$ is the complex conjugate of the data symbols carried in the sub-carrier $2K-1$ to $3K-1$. Thus, the non-uniform FFT matrix needs to be formed only in the data sub-carriers from $2K-1$ to $3K-1$.

Finally, the estimated signal is performed regarding the coarse Doppler compensation and fine phase correction as

$$\hat{\mathbf{Y}} = \tilde{\mathbf{Y}}[\mathbf{G}_{\mathbb{RS}}]. \tag{16}$$

After the Doppler shift is compensated by coarse and fine step, the received signal in the time domain is fed to the conventional 1-tab equalizer, to equalize the channel.

III. EXPERIMENT SETTING

The structure of our testbed is depicted in Fig. 6. As shown in this figure, the system is organized into three blocks including a transmitter block, a shallow-water environment, and a receiver block.

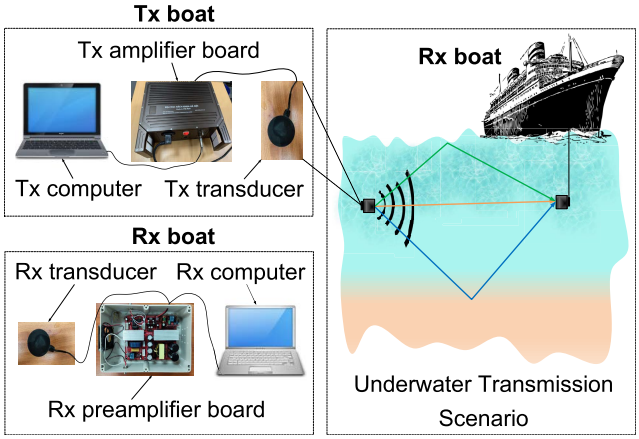

FIGURE 6. Transmission block diagram for digital underwater communication tests, transmitter(up) and receiver(bottom).

FIGURE 7. Sonar Amplifier made by Hanoi University of Science and Technology (HUST).

FIGURE 8. Transducer system installed on ship/float.

A. TRANSMITTER

- **Baseband Signal Processing** The baseband signal processing is performed with a laptop using Matlab to generate the data. The digital signal is converted into an analog signal by a built-in audio USB sound card and from it to the amplifier board. The sound card is used to generate the acoustic signal by sampling the analog signal at 96 kHz provided by the laptop.
- **Amplifier Board** In order to conduct a data transmission in underwater for a long distance, our team designed and built the acoustic power amplifier ourselves as shown in the Fig.7. Our power amplifier provides more than 500 watts of continuous power (1kW at DC). Frequency response is typically flat to within 0.071dB over an operated frequency range of 13.5kHz.
- **Transducer** After the digital-to-analog conversion, the modulated OFDM signal is amplified by the power amplifier, which is connected to the low-frequency acoustic transducer BII-7533 type 2 of the Benthowave company. The depth of the Tx transducer is approximately 10 m. The signal will be transmitted repeatedly to send a message to the receiver, which is responsible for decoding this message properly. Before transmitting an acoustic signal in the sea, or deep in the river, the proper adjustment of the impedance is extremely important, which determines the maximum output power of the transducer.

B. RECEIVER

The receiver block is depicted in Fig. 6. The receive side consists of a transducer, a preamplifier, and a computer, which performs the OFDM demodulation. The boat (Rx) acts as a receiver that is equipped with all these components. Rx transducer is also the BII-7533 type 2 with a depth ranging from 10m to 100m.

C. TRANSMISSION SCENARIOS

The measurement system is implemented on a number of rivers and lakes in Vietnam as shown in Fig. 9. Typical measurement locations are at Dong Do - lake[1], Hoa Binh - lake,[2] and Halong Bay, where measurement data is collected and processed. The underwater experiments were measured at a distance of 1km-1.5km with a straight line of sight (LOS), and the system parameters are described in Table 1.

The parameters of the experimental OFDM system are shown in Table 1, where the sampling frequency f_s is set to 96 kHz, and the frequency range of the system from 12 kHz to 15 kHz. We set the guard interval length of the 1024 sampling intervals, which ensures to mitigate ISI for the multi-path channel. The total number of sub-carriers is set to be $N_{\text{FFT}} = 2048$. The number of data sub-carriers and pilot sub-carriers are $N_d = 256$ and $N_p = 258$, respectively. The modulation scheme on each sub-carrier is QPSK.

[1]Dong Do Lake is an area of $0.6km^2$, $2km$ long and $20m$ deep.
[2]Hoa Binh lake is $208km^2$ wide, contains up to 9 billion m^3 of water, $100m$ deep.

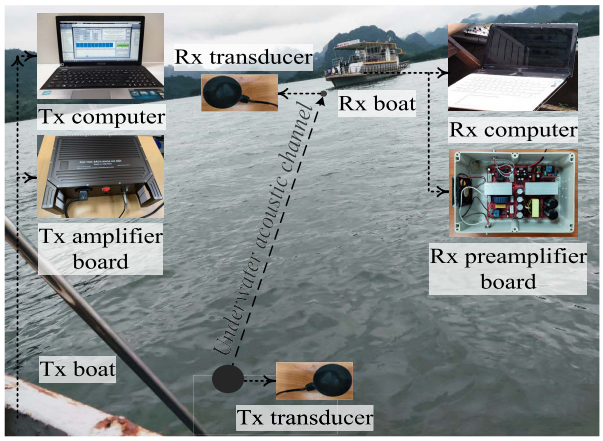

FIGURE 9. Photo of the measurement campaign in Halong Bay.

TABLE 1. System parameters.

Center frequency	$f_c = 13.5$ kHz
Signal Bandwidth	$B = 3$ kHz
OFDM block duration	$T_s = 32$ ms
Guard time	$T_g = 10.67$ ms
Sub-carrier spacing	$\Delta f = 46.875$ Hz
Modulation on each sub-carrier	QPSk
Number of sub-carrier	$N_{\mathrm{FFT}} = 2048$
Number of data sub-carrier	$N_d = 256$
Number of pilot sub-carrier	$N_p = 258$

Especially for underwater communications in bays or rivers there are many performance impacts which can be mentioned are 1) Because of the shallowness as well as the passage of boats, the surface waves affect the entire water area; 2) The bottom of rivers and seas where streams flow, often consists of mud and gas, causing undesirable effects on the signal; 3) The diverse reflections of rocks and walls (for Hoa Binh lake) cause significant spread over time.

In such practical transmission scenarios, it is found that in UWA transmission for several kilometers the coherence time of the sound channel is much shorter than the travel time of the signals between transceivers. Therefore, feedback of the CSI from the receiver to the transmitter is impractical. The reason is that the channel has changed at the time of receiving the data.

IV. RESULTS AND DISCUSSIONS

In this section, we provide the experiment's results to evaluate the effectiveness of our proposed Doppler compensation algorithm in UWA-OFDM. Table 2 shows Doppler frequency and normalized CFO of our system. Where the carrier frequency and the sub-carrier spacing are $f_c = 13.5$ kHz and $\Delta f = 46.875$ Hz, respectively. In water environment, the speed of sound is $c = 1500$ m/s. Thus, the maximum

TABLE 2. Doppler frequency and normalized CFO.

Carrier Frequency (f_c)	Subcarrier spacing (Δf)	Velocity (v)	Doppler frequency Max (f_d)	Normalized CF0 ϵ
13.5kHz	46.875Hz	2m/s	18Hz	0.384
13kHz [37]	9.53Hz	2m/s	17.33Hz	1.819
13.5kHz [38]	5.859Hz	2m/s	18Hz	3.072

Doppler frequency is $f_d = 18$ Hz and the normalized CFO is $\epsilon = 0.384$ when the relative motion velocity between two sides is $v = 2$ m/s. The parameters are decided based on actual observations, and are also consistent with other studies in [37], [38].

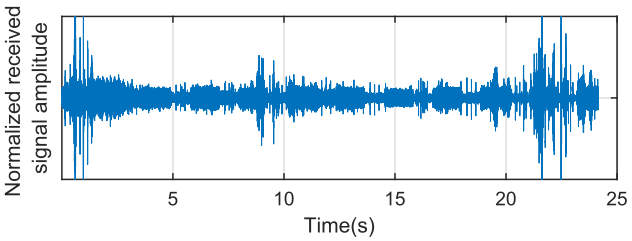

FIGURE 10. The received signal $y(n)$.

First, we discuss the received signal $y(n)$. As shown in Fig. 10, the total amount of time, which takes to receive a message, is 25 seconds. After an analog-to-digital converter (ADC) converts the received signal into a digital signal, we utilize a band-pass filter (BPF) to eliminate or attenuate frequencies both above and below the required frequency band.

Fig. 11 (a) depicts the spectrum of the received signal before filtering. The undesirable frequency in the received signal is removed using band-pass filtering, as shown in Fig. 11 (b). It can be observed in Fig. 11 (a) that the unexpected frequency's power is greater than PCF's power. This has a significant impact on the system's performance.

Secondly, a conventional ZP-OFDM is generated with the preamble duration of 10.67ms. The preamble is also designed to have remarkable peak correlation properties. The signal at the receiver is directly sampled with the system's hardware. A band-pass filtering is used to suppress the out-band noise of the received signal. Then time synchronization via a cross-correlation operation is performed to confirm the OFDM blocks have been transmitted correctly.

During the cross-correlation operation, a high peak occurs will appear, representing the preamble synchronization point. Fig. 12 represents the synchronous signals based on the designed preamble. For an underwater acoustic channel, the first arrived path may not be the strongest since underwater sound propagation has many different sources of reflections.

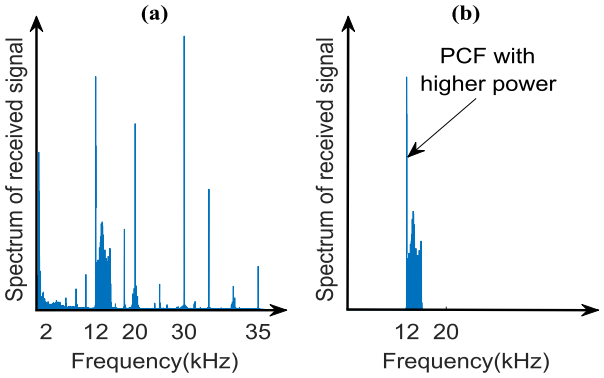

FIGURE 11. (a) The spectrum of the received signal and (b) The spectrum of the received signal after the bandpass filtering.

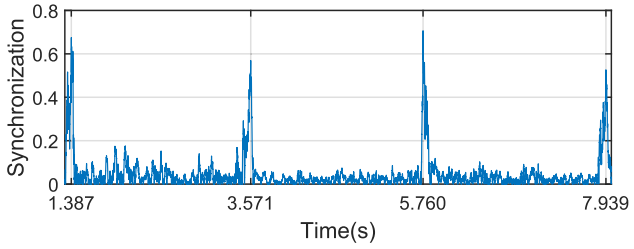

FIGURE 12. The synchronous signals based on preamble.

Algorithm 1 The Proposed OFDM Frame Synchronization Algorithm

Require: : $\mathbf{Y}(t)$ ▷ $\mathbf{Y}(t)$ is the received signal after the bandpass filtering

Ensure: : **SYN** ▷ **SYN** is the synchronization signal amplitude after applying the proposed algorithm

for $t \leftarrow 0$ to $t_{\max}$ **do** ▷ $t_{\max}$ is the total amount of time to receive a message
  $\mathbf{Y}_1 \leftarrow \mathbf{Y}(t \rightarrow t + T_g)$
  $\mathbf{Y}_2 \leftarrow \mathbf{Y}(t + T_s - T_g \rightarrow t + T_s)$
  $\mathbf{P}(t) = \sum_{t}^{t+T_g} |\mathbf{Y}_1 - \mathbf{Y}_2|$ ▷ $\mathbf{P}(t)$ the amplitude of the first synchronous signal
  Value $= \max(\mathbf{P}(t)) - \mathbf{P}(t)$ ▷ Value is the maximum value of the $\mathbf{P}(t)$ vector
  $\mathbf{P}(t) \leftarrow$ Value $- \mathbf{P}(t)$

  $\mathbf{R}(t) = \sum_{t}^{t+T_g} |\mathbf{Y}_1 \mathbf{Y}_2|$ ▷ $\mathbf{R}(t)$ the amplitude of the second synchronous signal
end for
SYN $= \mathbf{P}(t)\mathbf{R}(t)$
return SYN

These make synchronization problem difficult. Based on the time synchronization approach described above, the beginning point of each frame is detected based on the peak of cross-constellation process. Here we emphasize that in practice, how the timing offset affects on OFDM synchronization also needs to take into account in the particular environment and distance transmission. The proposed OFDM frame synchronization algorithm is described as in algorithm 1.

Fig. 13 (a) shows the transmitted signal designed as block-based OFDM frames. The timeout duration between two consecutive OFDM frames D_z is 0.875s. To interpret this setup, the choice of the length of the timeout period is based on the fact that the impulse response of the channel is highly variable in time. In the nearshore zone of the Bay of Halong, we have transmitted over 1.5 km distance, and the average transmission time is 0.875 seconds.

The signal received after the bandpass filter is shown in Fig. 13 (b) contains timeout periods, 10 complete OFDM frames and 2 incomplete OFDM frames at the beginning and end.

In the next step, we apply the above synchronization algorithm 1, to detect the beginning of 1 complete OFDM, as well as remove 2 OFDMs that have lost information at the beginning and at the end of the received signal. The result is shown in Fig. 13 (c), where the entire ten frames are filtered.

Fig. 13 (d) depicts the Dopper frequency variation in each sub-carriers over the entire OFDM frame. We clearly see that the Dopper varies strongly between sub-carriers. The Doppler shift correction is obtained by re-sampling the received signal, and interpolating re-sampled signal. However, the Doppler shift compensation in the coarse step is not enough to correct the phase distortion of the received PCF signal. Therefore, the study proposes to perform a fine-tuning step to deal with the phase distortion of the PCF signal based on the phase difference between two consecutive OFDM signals in a frame. The residual phase difference of the Doppler shift is alleviated by the non-uniform FFT technique. We then compare the performance of the system based on the BER metric in three cases as is shown in Fig. 14, specifically 1) the first case is without Doppler compensation; 2) the second is using the ICI matrix proposed in [39]; and 3) proposed Doppler frequency Compensation Matrix-based NFFT (DCMN). It is observed that the BER of DCMN and the BER in [39] are far better than the BER without Doppler compensation. It can be seen also the BER of DCMN is slightly better than that obtained by [39]. However, the system performance comparison based on the experiments is not always fair, since the experimental conditions are not identical. Moreover, the channel changes from time to time and also from experiment to experiment.The actual SNR level is unknown. Thus, the following section presents the system performance evaluation by numerical analysis and simulations.

V. PERFORMANCE EVALUATION BY NUMERICAL ANALYSIS AND SIMULATIONS

To justify the performance of the proposed method in comparision with the method in [39], we model the Doppler frequency by shifting the subcarrier frequency in an amount

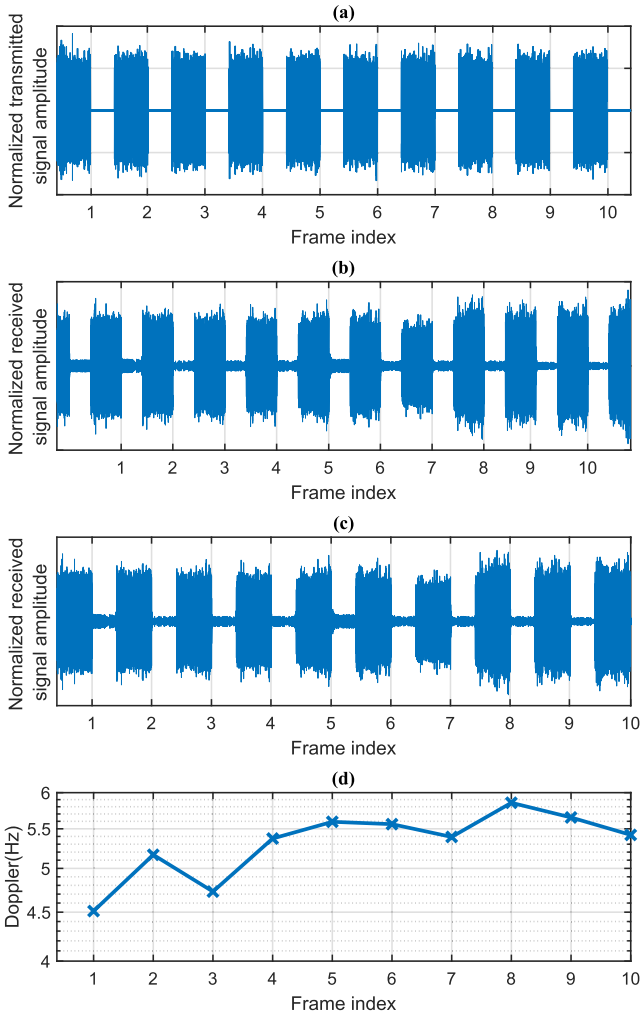

FIGURE 13. (a) The transmitted signal, (b) the received signal after the bandpass filtering, (c) the received signal captured by OFDM frame detecting and (d) the Dopper frequency variation in each frame.

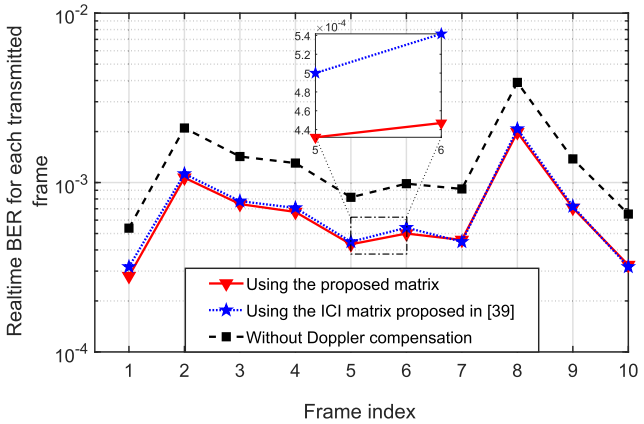

FIGURE 14. The Bit error rate of each frame.

of 12 Hz. The number of additions and multiplications of both methods are given in 3.

Compared with the method in [39], this study uses the useful data sub-carrier between $2K-1$ and $3K-1$ as shown in Figure 3. Then we use the non-uniform FFT matrix, that performs both the remaining Doppler frequency compensation and the FFT operation. Thus, the necessary additions and multiplications are significantly reduced.

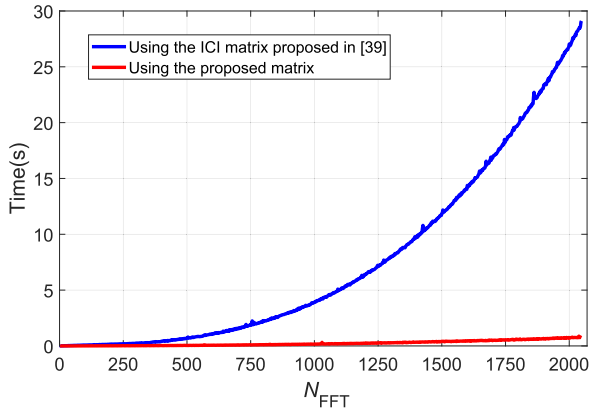

FIGURE 15. Comparing the complexity between two algorithms, one is proposed in [39] and the other is the proposed method.

TABLE 3. Complexity comparison.

	Proposed method	Method in [39]
Number of additions	$(N_{\text{FFT}-1}) \times K$	$(N_{\text{FFT}-1}) \times N_{\text{FFT}}$ $+N_{\text{FFT}} \log_2(N_{\text{FFT}})$
Number of multiplications	$N_{\text{FFT}} \times K$	N_{FFT}^2 $+N_{\text{FFT}}/2 \times \log_2(N_{\text{FFT}})$

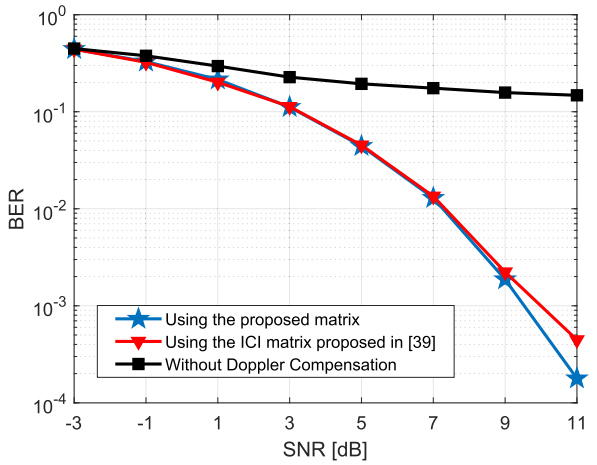

FIGURE 16. System performance comparision in terms of BER.

The benchmark based on the algorithmic processing time between [39] and this study is presented in Fig. 15. It can be seen that the proposed algorithm has significantly reduced complexity compared to [39].

Fig. 16 compares the system performance in terms of BER obtained by the proposed method with that one gained by the proposal in [39]. The case of without Doppler compensation is provided for reference. We can see that in the range of SNR higher than 9dB, our approach slightly outperforms the technique in [39].

VI. CONCLUSION

In this paper, we have proposed a parallel ICI canceling scheme via frequency shift compensation, which is designed based on non-uniform fast Fourier transform matrix (NFFT). This parallel scheme canceling scheme in frequency-domain equalizer aims to both compensate the Doppler phase shift and cancel the ICI. It is very well known, that the conventional one-tap equalizer has very high computational complexity because of the large matrix inversion problem. Therefore, we divide this high complexity equalizer problem into two sub-problems, and propose a coarse and fine Doppler frequency Compensation Matrix-based NFFT. By viewing the NFFT as a perturbed version of a uniform FFT, we address the major issue to generate the desired frequency response for the given filter specification, which is available in the actual underwater communication environment.

To evaluate the proposed method, we describes the design and testing in some actual underwater transmission environments with a transmission distance of about 1-1.5km.

The experimental results show that the proposed method can not only estimate the Doppler frequency shift by using the PCF, but also correct the phase distortion of the received signal. This help to improve the system performance regarding the ICI compensation. Complexity comparison also shows that the proposed method requires lower computation complexity than the state of the art. Our future research is to implement signal encoding methods to increase SINR for high speed communication applications.

REFERENCES

[1] B. Li, J. Huang, S. Zhou, K. Ball, M. Stojanovic, L. Freitag, and P. Willett, "MIMO-OFDM for high-rate underwater acoustic communications," *IEEE J. Ocean. Eng.*, vol. 34, no. 4, pp. 634–644, Oct. 2009.

[2] M. Murad, I. A. Tasadduq, and P. Otero, "Towards multicarrier waveforms beyond OFDM: Performance analysis of GFDM modulation for underwater acoustic channels," *IEEE Access*, vol. 8, pp. 222782–222799, 2020.

[3] T. H. Nguyen, T. V. Chien, H. Q. Ngo, X. N. Tran, and E. Bjornson, "Pilot assignment for joint uplink-downlink spectral efficiency enhancement in massive MIMO systems with spatial correlation," *IEEE Trans. Veh. Technol.*, vol. 70, no. 8, pp. 8292–8297, Aug. 2021.

[4] J.-K. Choi, H. N. Nguyen, T. H. Nguyen, H. Cho, H. K. Choi, and S. G. Park, "A time-domain estimation method of rapidly time-varying channels for OFDM-based LTE-R systems," *Digit. Commun. Netw.*, vol. 5, no. 2, pp. 94–101, May 2018.

[5] H. A. Le, T. Van Chien, T. H. Nguyen, H. Choo, and V. D. Nguyen, "Machine learning-based 5G-and-beyond channel estimation for MIMO-OFDM communication systems," *Sensors*, vol. 21, no. 14, p. 4861, Jul. 2021.

[6] I. A. Tasadduq, M. Murad, and P. Otero, "CPM-OFDM performance over underwater acoustic channels," *J. Mar. Sci. Eng.*, vol. 9, no. 10, p. 1104, Oct. 2021.

[7] V. Kuznetsov, K. Brazhenkova, D. Uvakin, P. Unru, and A. Rodionov, "Performance of the OFDM underwater acoustic communication system with high-rank subcarrier modulation and active beam pattern control," in *Proc. Global Oceans: Singap.—U.S. Gulf Coast*, Oct. 2020, pp. 1–5.

[8] Z. Kun, Q. S. Sen, K. T. Aik, and T. B. Aik, "A real-time coded OFDM acoustic modem in very shallow underwater communications," in *Proc. OCEANS—Asia Pacific*, May 2006, pp. 1–5.

[9] J. Wang, Y. Cui, H. Jiang, G. Pan, H. Sun, J. Li, and H. Esmaiel, "Estimation of Rice factor ratio for doubly selective fading channels," *IEEE Access*, vol. 8, pp. 31330–31340, 2020.

[10] J. Wang, Y. Cui, H. Sun, J. Li, M. Zhou, Z. A. H. Qasem, H. Esmaiel, and L. Liu, "Doppler shift estimation for space-based AIS signals over satellite-to-ship links," *IEEE Access*, vol. 7, pp. 76250–76262, 2019.

[11] T. Wang, J. G. Proakis, E. Masry, and J. R. Zeidler, "Performance degradation of OFDM systems due to Doppler spreading," *IEEE Trans. Wireless Commun.*, vol. 5, no. 6, pp. 1422–1432, Jun. 2006.

[12] A. Bourre, S. Lmai, C. Laot, and S. Houcke, "A robust OFDM modem for underwater acoustic communications," in *Proc. MTS/IEEE OCEANS—Bergen*, Jun. 2013, pp. 1–5.

[13] M. Murad, I. A. Tasadduq, and P. Otero, "Pilot-assisted OFDM for underwater acoustic communication," *J. Mar. Sci. Eng.*, vol. 9, no. 12, p. 1382, Dec. 2021.

[14] R. Hegazy, J. Kadifa, L. Milstein, and P. Cosman, "Subcarrier mapping for underwater video transmission over OFDM," *IEEE J. Ocean. Eng.*, vol. 46, no. 4, pp. 1408–1423, Oct. 2021.

[15] X. Wang, X. Wang, R. Jiang, W. Wang, Q. Chen, and X. Wang, "Channel modelling and estimation for shallow underwater acoustic OFDM communication via simulation platform," *Appl. Sci.*, vol. 9, no. 3, p. 447, Jan. 2019.

[16] A. L. Ha, T. Van Chien, T. H. Nguyen, W. Choi, and V. D. Nguyen, "Deep learning-aided 5G channel estimation," in *Proc. 15th Int. Conf. Ubiquitous Inf. Manage. Commun. (IMCOM)*, Jan. 2021, pp. 1–7.

[17] Y. Wu, Y. Yao, N. Wang, and M. Zhu, "Deep learning-based timing offset estimation for deep-sea vertical underwater acoustic communications," *Appl. Sci.*, vol. 10, no. 23, p. 8651, Dec. 2020.

[18] M. R. Khan, B. Das, and B. B. Pati, "Channel estimation strategies for underwater acoustic (UWA) communication: An overview," *J. Franklin Inst.*, vol. 357, no. 11, pp. 7229–7265, Jul. 2020.

[19] M. Morelli and U. Mengali, "A comparison of pilot-aided channel estimation methods for OFDM systems," *IEEE Trans. Signal Process.*, vol. 49, no. 12, pp. 3065–3073, Dec. 2001.

[20] A. Zhao, C. Zeng, J. Hui, K. Wang, and K. Tang, "Study on time reversal maximum ratio combining in underwater acoustic communications," *Appl. Sci.*, vol. 11, no. 4, p. 1509, Feb. 2021.

[21] Y. Xie, X. Hu, J. Xiao, D. Wang, and W. Lei, "Implementation of timing synchronization for OFDM underwater communication system on FPGA," in *Proc. 3rd Int. Conf. Anti-Counterfeiting, Secur., Identificat. Commun.*, Aug. 2009, pp. 568–570.

[22] C. Krishnaswamy, T. Chinnasamy, V. Gowthaman, S. Narayanan, T. Sudhakar, and M. Atmanand, "Underwater communication implementation with OFDM," *Indian J. Geo-Mar. Sci.*, vol. 44, no. 2, pp. 259–266, 2015.

[23] L. Songzuo, M. Lu, L. Hui, C. Tingting, and Q. Gang, "Design and implementation of OFDM underwater acoustic communication algorithm based on OMAP-L138," in *Proc. Int. Conf. Underwater Netw. Syst. (WUWNET)*. New York, NY, USA: Assoc. Comput. Machinery, 2014, pp. 1–5.

[24] T. Dean, M. Chowdhury, and A. Goldsmith, "Zero-padded FDM-FDCP: Real-time signal processing for underwater channels," in *Proc. IEEE 19th Int. Workshop Signal Process. Adv. Wireless Commun. (SPAWC)*, Jun. 2018, pp. 1–5.

[25] B. Muquet, Z. Wang, G. B. Giannakis, M. D. Courville, and P. Duhamel, "Cyclic prefixing or zero padding for wireless multicarrier transmissions?" *IEEE Trans. Commun.*, vol. 50, no. 12, pp. 2136–2148, Dec. 2002.

[26] Z. Wang, S. Zhou, G. B. Giannakis, C. R. Berger, and J. Huang, "Frequency-domain oversampling for zero-padded OFDM in underwater acoustic communications," *IEEE J. Ocean. Eng.*, vol. 37, no. 1, pp. 14–24, Jan. 2012.

[27] E. Demirors, G. Sklivanitis, T. Melodia, G. E. Santagati, and S. N. Batalama, "A high-rate software-defined underwater acoustic modem with real-time adaptation capabilities," *IEEE Access*, vol. 6, pp. 18602–18615, 2018.

[28] A. Radosevic, R. Ahmed, T. Duman, J. Proakis, and M. Stojanovic, "Adaptive OFDM modulation for underwater acoustic communications: Design considerations and experimental results," *IEEE J. Ocean. Eng.*, vol. 39, no. 2, pp. 357–370, Apr. 2013.

[29] I. Nissen, "Pilot-based OFDM-systems for underwater communication applications," in *Proc. Conf. New Concepts Harbour Protection, Littoral Secur. Underwater Acoustic Commun.*, 2005, pp. 1–8.

[30] M. M. Yüksel, "Underwater acoustic modem using OFDM," M.S. thesis, Bilkent Univ., Ankara, Turkey, 2012.

[31] P. A. van Walree, "Propagation and scattering effects in underwater acoustic communication channels," *IEEE J. Ocean. Eng.*, vol. 38, no. 4, pp. 614–631, Oct. 2013.

[32] G. Qiao, Z. Babar, L. Ma, S. Liu, and J. Wu, "MIMO-OFDM underwater acoustic communication systems—A review," *Phys. Commun.*, vol. 23, pp. 56–64, Jun. 2017.

[33] B. Li, S. Zhou, M. Stojanovic, L. Freitag, and P. Willett, "Multicarrier communication over underwater acoustic channels with nonuniform Doppler shifts," *IEEE J. Ocean. Eng.*, vol. 33, no. 2, pp. 198–209, Apr. 2008.
[34] T. MinhHai, S. Rie, S. Taisuki, and T. Wada, "A transceiver architecture for ultrasonic OFDM with adaptive Doppler compensation," in *Proc. OCEANS—MTS/IEEE Washington*, Oct. 2015, pp. 1–6.
[35] J. Meng, H. Wang, P. Ye, Y. Zhao, L. Guo, H. Zeng, and Y. Tian, "I/Q linear phase imbalance estimation technique of the wideband zero-IF receiver," *Electronics*, vol. 9, no. 11, p. 1787, Oct. 2020.
[36] P. H. Moose, "A technique for orthogonal frequency division multiplexing frequency offset correction," *IEEE Trans. Commun.*, vol. 42, no. 10, pp. 2908–2914, Oct. 1994.
[37] W. Zhou, Z. Wang, J. Huang, and S. Zhou, "Blind CFO estimation for zero-padded OFDM over underwater acoustic channels," in *Proc. OCEANS MTS/IEEE KONA*, Sep. 2011, pp. 1–7.
[38] G. Avrashi, A. Amar, and I. Cohen, "Time-varying carrier frequency offset estimation in OFDM underwater acoustic communication," *Signal Process.*, vol. 190, Jan. 2022, Art. no. 108299.
[39] Q. K. Nguyen, D. H. Do, and V. D. Nguyen, "Doppler compensation method using carrier frequency pilot for OFDM-based underwater acoustic communication systems," in *Proc. Int. Conf. Adv. Technol. Commun. (ATC)*, Oct. 2017, pp. 254–259.

VAN DUC NGUYEN was born in Thanh Hoa, Vietnam, in 1973. He received the B.E. and M.E. degrees in electronics and communications from the Hanoi University of Technology, Vietnam, in 1995 and 1997, respectively, and the Dr.Eng. degree in communications engineering from the University of Hannover, Germany, in 2003. From 1995 to 1998, he was an Assistant Researcher with the Technical University of Hanoi. In 1996, he participated in the Student Exchange Program between the Technical University of Hanoi and the Munich University of Applied Sciences for one term. From 1998 to 2003, he was with the Institute of Communications Engineering, University of Hannover, first as a DAAD Scholarship Holder and then as a Member of the Scientific Staff. From 2003 to 2004, he was a Postdoctoral Researcher with the Agder University College, Grimstad, Norway. He was a Postdoctoral Fellow with the International University of Bremen. He devoted three years at Sungkyunkwan University, Klagenfurt University, and Agder University, as a Visiting Professor. His current research interests include mobile radio communications, especially MIMO-OFDM systems, and radio resource management, channel coding for cellular, and ad-hoc networks.

HOAI LINH NGUYEN THI received the B.S. degree in electronic and telecommunication from the Hanoi University of Science and Technology (HUST), Hanoi, Vietnam, in 2021, where she is currently pursuing the master's degree in telecommunication engineering.

QUOC KHUONG NGUYEN received the B.S., M.Sc., and Ph.D. degrees in electronics and telecommunications engineering from the Hanoi University of Science and Technology (HUST), Hanoi, Vietnam, in 1995, 1997, and 2011, respectively. He is currently working with the Department of Communications Engineering, HUST, as a Lecturer. His research interests include signal processing for wireless communications, MIMO-OFDM, and underwater communication systems.

TIEN HOA NGUYEN received the Dipl.-Ing. degree in electronics and communication engineering from Hannover University. He has worked with the Research and Development Department of image processing and the Development of SDR-Based Drivers, Bosch, Germany. He devoted three years of experimentation with MIMOon's Research and Development Team to develop embedded signal processing and radio modules for LTE-A/4G. He worked as a Senior Expert at the Viettel IC Design Center (VIC) and VinSmart for development of advanced solutions at the PHY layer in 5G systems. He is currently a Lecturer at the School of Electronics and Telecommunications, Hanoi University of Science and Technology. His research interests include resource allocation in B5G/6G, massive MIMO, and vehicular communication systems.